Swimming ghosts of the halophilic archaeon, *Haloferax volcanii*

Yoshiaki Kinosita[1,2], Nagisa Mikami[2], Zhengqun Li[2], Frank Braun[2], Tessa EF. Quax[2], Chris van der Does[2], Robert Ishmukhametov[1], Sonja-Verena Albers[2] & Richard Berry[1]

[1]Department of Physics, University of Oxford, Park load OX1 3PU, Oxford, UK

[2]Institute for Biology II, University of Freiburg, Schaenzle strasse 1, 79104, Freiburg, Germany

Correspondence should be addressed to richard.berry@physics.ox.ac.uk

Author Contributions:

Y.K. and R.B designed the research. Y.K. performed all experiments and obtained all data; N.M. helped genetics, biochemistry, and preparation of figures; Z.L, F.B., T.EF.Q., C.v.d.D and S.-V. A. helped genetics; R.I helped the ghost experiments; N.M. and R.B helped microscope measurements; Y.K., and R.B. wrote the paper.

Abstract

Archaea swim driven by a membrane-embedded rotary machine, the archaellum. Current understanding of the archaellar motor complex is limited by the lack of a versatile model system for its experimental study. Here we establish a membrane permeabilized ghost-cell model which enables control and quantification of ATP-coupled archaellar rotation. We find a high nucleotide selectivity for rotation and no cooperativity which is a different characteristic of *in vitro* studies.

Microorganisms exhibit various types of motilities, such as gliding, swimming, and twitching, driven by supramolecular motility machinery composed of multiple different proteins [1]. In archaea, cells swim driven by rotation of an archaellum (archaeal flagellum) which consists of a torque-generating motor and a helical filament which acts as a propeller (Fig. 1a) [2]. The archaellum is no homologous to any bacterial flagellum protein but is evolutionarily and structurally related to bacterial type IV pili for a surface motility. In Euryarchaeota, the filament encodes in two genes, *flgA (flaA in Methanococcus)* or *flgB (flaB in Methanococcus)*, and the motor nine *fla*C-K (see Ref. 2 for details in Crenarchaeota). Furthermore, some Euryarchaeota possess chemotactic proteins, such as CheY for a response regulator and CheF as an archaeal specific adaptor protein, which might have been acquired by horizontal gene transfer from bacteria [3]. Figure 1a shows the current association of functions with the motor genes, based on analysis of mutants and biochemical data: FlaC/D/E as switching proteins for the directional switch of the archaellum rotation coupled with the signals from the chemotaxis system [4]; FlaG and FlaF as a stator interacting with the surface layer (S-layer) with FlaF regulating FlaG filament assembly [5, 6]; FlaH regulates the switch between assembly of the archaella and rotation [2]; FlaI as the ATP-driven motor for both archaella assembly and rotation [7]; FlaJ is the membrane protein; and FlaK/PibD as the pre-archaellin peptidase [8]. An inhibitor of proton translocating ATP synthases reduced both intracellular [ATP] and swimming speed in *Halobacterium salinarum*, suggesting that archaellar rotation is driven by ATP [9]. However, direct evidence is still lacking, and reconstituted systems to directly manipulate and investigate the motor complex are also missing.

51 Here we present an *in vitro* system for the archaellum, similar to the Triton model for
52 the eukaryotic flagellum [10] and the permeabilized ghost model for gliding *Mycoplasma*
53 *mobile* [11, 12]. We use the halophilic archaeon *Haloferax volcanii* [13]. *Hfx. volcanii*
54 possesses multiple polar archaella and swims at 2-5 μm s^{-1} at room temperature, with CW
55 rotation more efficient for propulsion than CCW (Supplementary Result 1 and
56 Supplementary Movie 1) [14]. We increased the fraction of swimming *Hfx. volcanii* cells
57 from 20-30 % [13] to 80 % by adding 20 mM $CaCl_2$ (Fig. S1a).
58 To prepare our experimental model system, we suspended motile cells in buffers
59 containing 0.15 % sodium cholate and 2.5 mM ATP (Fig. 1c). Fluorescent imaging
60 revealed that ghosts still possessed archaellar filaments, the cell membrane, and S-layer
61 (Fig. 1b bottom and Fig. S3). The detergent reduced the refractive index of cells,
62 indicating permeabilization of the cell membrane and corresponding loss of cytoplasm.
63 Remarkably, the permeabilized cells still swam (Supplementary Movie 2 and Fig. 1c
64 *lower right*). We named them "ghosts," as in similar experiments on *Mycoplasma mobile*
65 [12]. Fig. 1d shows a typical example of a live swimming cell changing to a ghost, marked
66 by a sudden change of image density at 8.75 sec. In a solution containing 2.5 mM ATP,
67 the swimming speed did not change dramatically (Fig. 1e, see Fig. S4a for another
68 example). Fig. 1f shows histograms of swimming speed before and after adding detergent.
69 The average and SD were 1.79 ± 0.38 μm s^{-1} before and 1.55 ± 0.42 μm s^{-1} after
70 permeabilization (P = 0.421834>0.05 by t-test, ratio 0.93 ± 0.24, n = 24, Fig. S4b),
71 indicating that ghosts swim at the same speed as live cells in this, saturating, ATP
72 concentration. The single speed peak, unlike Fig. S1b, might indicate a lack of CW
73 rotation in these swimming cells in presence of detergent (Fig. 1f). However, we found it

74 difficult to track swimming ghosts due to their low contrast, and were not able to
75 determine the direction of archaellar rotation.
76 To overcome these difficulties, we established a ghost-bead assay for measuring ATP-
77 coupled motor rotation (Fig. 2a). We attached cells with biotinylated archaellar filaments
78 nonspecifically to the cover glass surface, and then introduced streptavidin beads (500
79 nm or 1000 nm diameter) which attached to the filaments (Supplementary Method and
80 Results 2). Addition of 0.1 mg ml^{-1} streptavidin (which would crosslink adjacent filaments
81 in a rotating bundle) did not stop bead rotation, indicating that beads are rotated by a
82 single motor [15] (Supplementary movie 3). For the preparation of ghosts, live cells
83 labelled with rotating beads were treated with 0.3 % sodium cholate for less than 30 sec
84 to permeabilize their cell membrane in a flow chamber, and subsequently the detergent
85 was replaced with buffer containing ATP (Supplementary movie 4 and Fig. 2b). Motor
86 rotation was stopped by permeabilization and reactivated by the addition of ATP. Beads
87 on ghost cells rotated in both directions (see Supplementary Results 3). However, we did
88 not see any differences in rotation rates under various ATP concentrations and therefore
89 analyzed speeds collectively. Beads on live cells with CheY deleted showed a reduced
90 probability of CW rotation: 6% showed some CW rotation during 30s observation,
91 compared to 37% in the wild-type. Switching was very rare: 15% of wild-type and no
92 *ΔcheY* cells switched during 30s recordings (Supplementary table 3). Wild type ghost still
93 exhibits switching, but the bias and fraction of CW/CCW/switching were slightly
94 changed, suggesting the chemotaxis system still active, although not entirely. Note that
95 our finding that archaeal CheY controls CW bias in a motor rotation is inconsistent with
96 a previous report (see details in Supplementary Result 4) [16].

97 We then investigated the effect of nucleotides on rotation using 500-nm beads. First, we
98 checked the nucleotide selectivity of rotation. Previous bulk experiments showed that
99 purified FlaI could hydrolyze different nucleotide triphosphates (NTPs) at similar rates
100 [17]. However, the rotational rates of 500 nm beads on ghosts in 10 mM GTP, CTP, and
101 UTP in ghost experiments were 5-10 times slower than in ATP (Fig. 2c). This suggests
102 that the motor complex might increase the selectivity of FlaI for nucleotides and/or
103 prevent extra energy consumption *in vivo* like the endopeptidase Clp (see Fig. 1B in [18]).
104 Second, we examined the ATP-dependence of rotation of the range of 8 μM to 10 mM
105 [ATP] (Figure 2d and Supplementary movie 5). Rotation speeds followed simple
106 Michaelis-Menten kinetics, with V_{max} 7.14 Hz and K_m, 284 μM (n = 452; Fig. 2d red). A
107 fit with the Langmuir-Hill equation showed no cooperativity in ATP turnover (Hill
108 coefficient 0.85) consistent with previous measurements of purified FlaI [19]. Finally, we
109 found that ATP-γ-S, ADP, and ADP+Pi inhibited motor rotation as competitive inhibitors,
110 showing that the rotation is driven by the hydrolysis of ATP into ADP+ Pi (Supplementary
111 Results 6). We furthermore examined the effects of detergent, pH, and ion concentration
112 on rotation (Supplementary Results 7-8).
113 We then examined ATP-dependent rotation using 1000-nm beads (Supplementary movie
114 6). Rotation speeds again obeyed simple Michaelis-Menten kinetics, with V_{max}, K_m, and
115 Hill coefficient estimated to be 2.79 Hz, 161 μM, and 0.79 (n = 189; Fig. 2d blue). We
116 estimated motor torques of 180.83 ± 43.06 pN nm for live cells (Fig. 2e *top*, n = 72) and
117 151.10 ± 27.23 pN nm for ghosts at 10 mM [ATP] (Fig. 2e *bottom*, n = 46), using $T =$
118 $2\pi f\xi$, where f is rotation speed and ξ the viscous drag coefficient of the bead (See
119 Supplementary Methods). These values are in good agreement with previous
120 measurements of *Hbt. salinarum* live cells [20]. By contrast we estimated motor torques

121 approximately 100 pN nm when driving 500-nm beads, suggesting a speed-dependence
122 of torque in *Hfx. volcanii* motor which is similar to the bacterial flagellar motor [21] but
123 different from the *Hbt. salinarum* archaellar motor [20] (Supplementary Result 9). We
124 also observed one instance of a sudden change in the speed of a motor during long-term
125 observation (Fig. S13), similar to speed changes attributed to load-dependent structural
126 dynamics of the bacterial flagellar motor [22, 23].

127 As previously for *Hbt. salinarum* [20], our measured torque requires by conservation of
128 energy the hydrolysis of ~12 ATP molecules to drive a single rotation of a motor labelled
129 with a 1000 nm bead. That paper proposed a model of motor rotation driven by multiple
130 ATP molecules per mechanochemical cycle of the 6-fold FlaI ATPase, to reconcile this
131 contradiction; however, our ghost data indicate no cooperativity in ATP hydrolysis for
132 rotation (Fig. 2d). To address this paradox, we need to measure and analyse the stepping
133 patterns of archaellar rotation. If dwell times between steps show a single or double
134 exponential distribution, this would be consistent with stochastic reaction kinetics and no
135 cooperativity, as seen in F_1-ATPase [24]. On the other hand, a coordinated chemical cycle
136 between dwell and burst phases as seen in bacteriophage φ29 [25] is another possibility.
137 Our ghost-cell model system will allow us to address the above paradox and understand
138 the torque generation mechanism at the single-molecule level.

139 The ghost technique also has the potential for application to other biological systems.
140 Archaea display chemotactic [3] and cell division machineries [26] acquired by horizontal
141 gene transfer from bacteria. Although the archaellum and bacterial flagellum are
142 completely different motility systems, they share common chemotactic proteins. In
143 principle, the effect of chemotactic proteins from different hosts on motor switching could
144 be monitored by combing ghost cells and purified proteins. Similarly, our ghost cells offer

the potential to manipulate and study the archaeal cell division machinery as with *in vitro* ghost models of *Schizosaccharomyces pombe* [27]. Ghost archaea offer the advantages of both *in vivo* and *vitro* experimental methods, and will allow the exploration of the universality, diversity, and evolution of biomolecules in microorganisms.

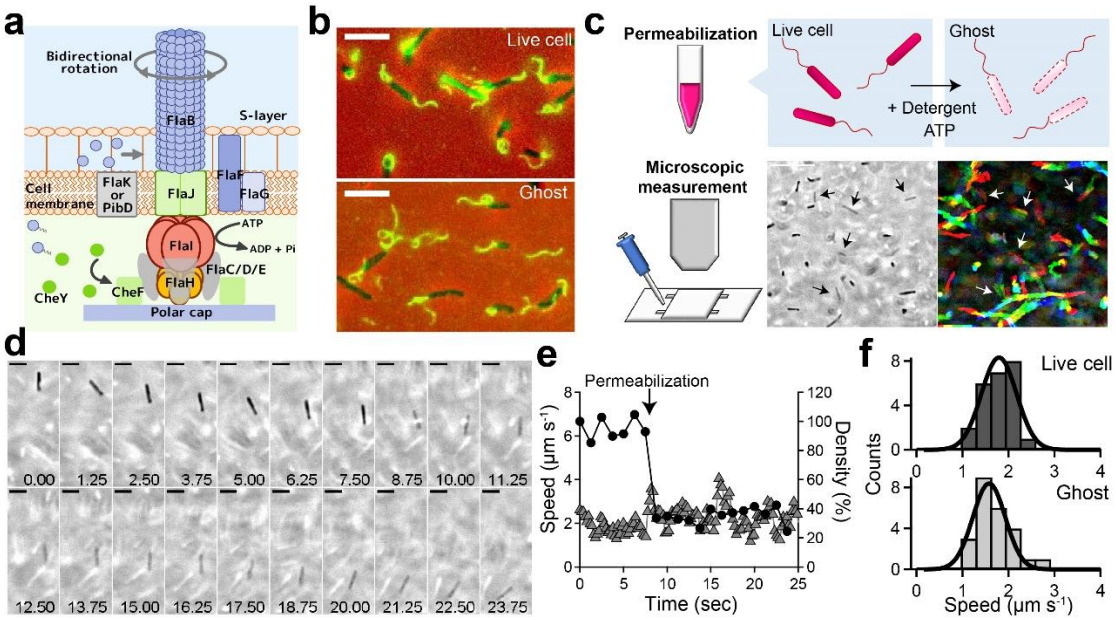

Figure 1 Swimming ghosts

(a) The current model of archaeal motor in Euryarchaeota. Details were described in the main text. (b) Merge image of live cells (*top*) and ghosts (*bottom*) labeled with a streptavidin dylight488 which binds to biotinylated cells. (c) Procedures to observe swimming ghosts. Live cells were permeabilized in a tube, then induced into a flow chamber to observe swimming motility. *Lower middle*: Phase-contrast image. Black arrows indicate ghosts. Scale bar, 10 μm. Lower right: The sequential images with 0.5-s intervals were integrated for 30 sec with the intermittent color code "red → yellow → green → cyan → blue." White arrows indicate trajectories of ghosts. (d) Sequential images of change from a live cell to ghost. Scale bar, 5 μm. (e) Time course of a swimming speed (*v*, triangles) and cell density (circles) of (d). Arrow indicates the time of permeabilization. (f) Histogram of a swimming speed, where the average and SD were 1.79 ± 0.38 μm s^{-1} before permeabilization (live cells) and 1.55 ± 0.42 μm s^{-1} after permeabilization (ghosts), respectively (n = 24).

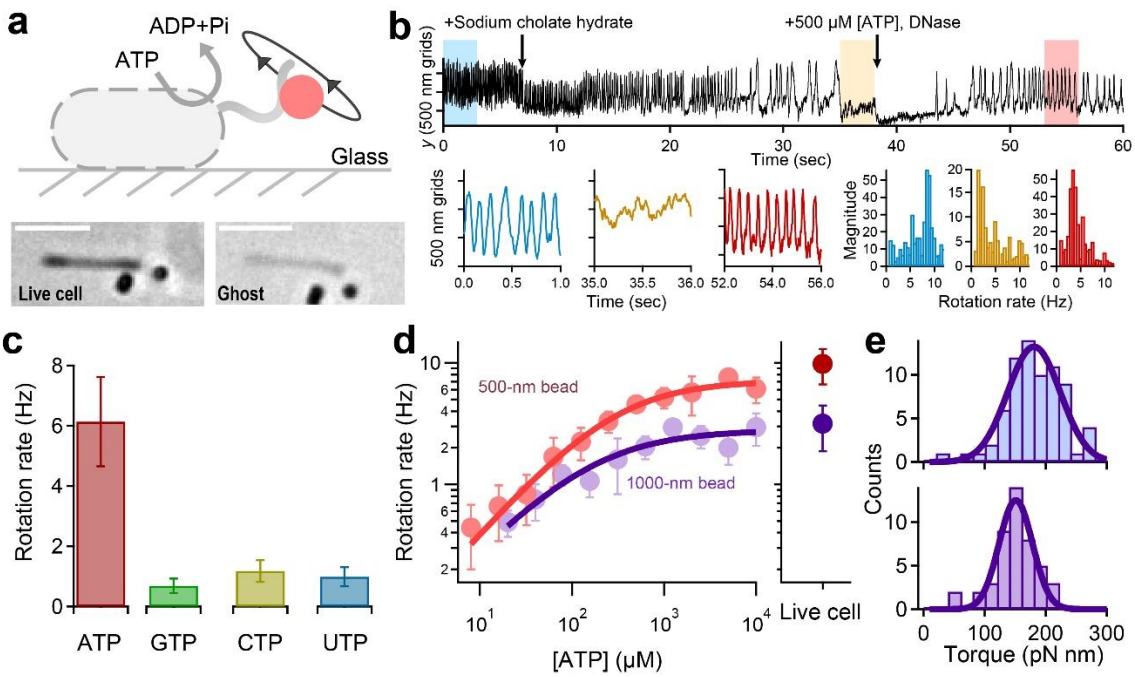

Figure 2 Visualization of a motor rotation of ghost through a bead rotation attached to an archaellar filament.

(a) The schematics of an experimental setup (*top*) and a phase-contrast image of live cell (*lower left*) and ghost (*lower right*). Scale bar, 5 μm. (b) *Top*: Time course of *y*-trace during ghost preparations, each color section corresponds to *y*-time traces (*lower left*) and Fourier transform analysis (*lower right*). At the blue section, a live cell exhibited a bead rotation, and then motor rotation after treatment with 0.3 % sodium cholate became gradually slow or almost stopped at an orange section. After the addition of ATP, the motor was reactivated and exhibited rotation again. Data from Supplementary movie 4. (c) Rotation rate at 10 mM [NTP]. The average and SD were 6.14 ± 1.48 Hz for ATP (n = 47), 0.69 ± 0.24 Hz for GTP (n = 30), 1.18 ± 0.36 Hz for CTP (n = 32), and 0.99 ± 0.32 Hz for UTP (n = 29), respectively, (d) *Left*: The rotation rate of 500 nm bead (red) and 1000 nm bead (blue) attached to an archaellar filament at different [ATP]s in

181 solution. The solid lines show a fit with Hill-Langmuir equation $\frac{V_{max}\times[ATP]^n}{{K_m}^n+[ATP]^n}$; where

182 V_{max}, K_m and n are 7.14 Hz, 284 μM, and 0.85 for 500 nm bead (n = 452), and

183 2.79 Hz, 161 μM, and 0.79 for 1000 nm bead (n = 189) respectively. Right: The

184 rotation rate of live cells, where the average and SD were 10.17 ± 2.39 Hz for

185 500 nm bead (n = 32) and 3.16 ± 1.29 Hz for 1000 nm bead (n = 62). (e)

186 Histograms of torque using a 1000 nm bead, where the average and SD were

187 180.83 ± 40.36 pN nm for live cells (*top*, n = 72) 151.10 ± 27.23 pN nm (*bottom*,

188 n = 46) for ghosts, (P = 0.0001<0.05 by *t*-test).

189

Acknowledgements

We thank Dr. Abhishek Mazumder and Prof. Achillefs Kapanidis for sharing chemicals, and Dr. Mitsuhiro Sugawa for technical advice in the microscope measurement. This study was supported in part by a grant from the Funding Program for the Biotechnology and Biological Sciences Research Council (to R.M.B), Collaborative Research Center Grant from the Deutsche Forschungsgemeinschaft (to S-V.A.). Y.K was recipient of the Japan Society for the Promotion of Science Postdoctoral Fellowship for Research Abroad and the Uehara Memorial Foundation postdoctoral fellow, and N.M was recipient of the Yoshida Scholarship Foundation.

Conflict of interest

The authors declare no competing financial interests.

Supplementary methods

Supplementary Results 1-9

Supplementary Figures 1-14

Supplementary Table 1-3

Captions for Supplementary Movies

References

References

[1] Jarrell, K. F. & McBride, M. J. (2008) *Nat Rev Microbiol* **6:**466-476

[2] Albers, S. V. & Jarrell, K. F. (2018) *Trends Microbiol* **26:**351-362

[3] Briegel, A., Ortega, D. R., Huang, A. N.*, et al.* (2015) *Environ Microbiol Rep* **7:**414-419

[4] Schlesner, M., Miller, A., Streif, S.*, et al.* (2009) *BMC Microbiol* **9:**56

[5] Banerjee, A., Tsai, C. L., Chaudhury, P.*, et al.* (2015) *Structure* **23:**863-872

[6] Tsai, C. L., Tripp, P., Sivabalasarma, S.*, et al.* (2020) *Nat Microbiol* **5:**216-225

[7] Reindl, S., Ghosh, A., Williams, G. J.*, et al.* (2013) *Mol Cell* **49:**1069-1082

[8] Hu, J., Xue, Y., Lee, S.*, et al.* (2011) *Nature* **475:**528-531

[9] Streif, S., Staudinger, W. F., Marwan, W.*, et al.* (2008) *J Mol Biol* **384:**1-8

[10] Gibbons, B. H. & Gibbons, I. R. (1972) *J Cell Biol* **54:**75-97

[11] Kinosita, Y., Nakane, D., Sugawa, M.*, et al.* (2014) *Proc Natl Acad Sci U S A* **111:**8601-8606

[12] Uenoyama, A. & Miyata, M. (2005) *Proc Natl Acad Sci U S A* **102:**12754-12758

[13] Quax, T. E. F., Altegoer, F., Rossi, F.*, et al.* (2018) *Proc Natl Acad Sci U S A* **115:**E1259-E1268

[14] Kinosita, Y., Uchida, N., Nakane, D.*, et al.* (2016) *Nat Microbiol* **1:**16148

[15] Berg, H. C. & Anderson, R. A. (1973) *Nature* **245:**380-382

[16] Rudolph, J. & Oesterhelt, D. (1996) *J Mol Biol* **258:**548-554

[17] Ghosh, A., Hartung, S., van der Does, C.*, et al.* (2011) *Biochem J* **437:**43-52

[18] Ripstein, Z. A., Vahidi, S., Houry, W. A.*, et al.* (2019) *bioRxiv* 780494

[19] Chaudhury, P., van der Does, C., & Albers, S. V. (2018) *PeerJ* **6:**e4984

[20] Iwata, S., Kinosita, Y., Uchida, N.*, et al.* (2019) *Commun Biol* **2:**199

[21] Ryu, W. S., Berry, R. M., & Berg, H. C. (2000) *Nature* **403:**444-447

[22] Lele, P. P., Hosu, B. G., & Berg, H. C. (2013) *Proc Natl Acad Sci U S A* **110:**11839-11844

[23] Tipping, M. J., Delalez, N. J., Lim, R.*, et al.* (2013) *MBio* **4:**

[24] Yasuda, R., Noji, H., Yoshida, M.*, et al.* (2001) *Nature* **410:**898-904

[25] Moffitt, J. R., Chemla, Y. R., Aathavan, K.*, et al.* (2009) *Nature* **457:**446-450

[26] Makarova, K. S., Yutin, N., Bell, S. D.*, et al.* (2010) *Nat Rev Microbiol* **8:**731-741

[27] Mishra, M., Kashiwazaki, J., Takagi, T.*, et al.* (2013) *Nat Cell Biol* **15:**853-859